

Omni-DNA: A Unified Genomic Foundation Model for Cross-Modal and Multi-Task Learning

Zehui Li^{1,2} Vallijah Subasri^{3,4} Yifei Shen¹ Dongsheng Li¹ Yiren Zhao² Guy-Bart Stan² Caihua Shan¹

Abstract

Large Language Models (LLMs) demonstrate remarkable generalizability across diverse tasks, yet genomic foundation models (GFMs) still require separate finetuning for each downstream application, creating significant overhead as model sizes grow. Moreover, existing GFMs are constrained by rigid output formats, limiting their applicability to various genomic tasks. In this work, we revisit the transformer-based auto-regressive models and introduce Omni-DNA, a family of cross-modal multi-task models ranging from 20 million to 1 billion parameters. Our approach consists of two stages: (i) **pretraining** on DNA sequences with next token prediction objective, and (ii) **expanding** the multi-modal task-specific tokens and **finetuning** for multiple downstream tasks simultaneously. When evaluated on the Nucleotide Transformer and GB benchmarks, Omni-DNA achieves state-of-the-art performance on 18 out of 26 tasks. Through multi-task finetuning, Omni-DNA addresses 10 acetylation and methylation tasks at once, surpassing models trained on each task individually. Finally, we design two complex genomic tasks, *DNA2Function* and *Needle-in-DNA*, which map DNA sequences to textual functional descriptions and images, respectively, indicating Omni-DNA’s cross-modal capabilities to broaden the scope of genomic applications. All the models are available through <https://huggingface.co/collections/zehuil27>.

1. Introduction

The volume of genomic data has been increasing at an exponential rate over the past decades (Lathe et al., 2008), making it infeasible to annotate these sequences manually.

¹Microsoft Research ²Imperial College London ³Vector Institute ⁴University Health Network. Correspondence to: Zehui Li <zl6222@ic.ac.uk>, Caihua Shan <cai-hua.shan@microsoft.com>.

Model Input: What is the function of this sequence?GGCTG...TTTTCTGA

Ground Truth: Olfactory receptor 5A2-like (OR5A2L) is a member of the olfactory receptor gene family, which is involved in the detection of volatile substances, contributing to the sense of smell.

Omni-DNA: The mRNA for olfactory receptor family 5 subfamily B member 109 (OR5B109) encodes a protein that is part of the olfactory receptor family. These receptors are involved in the detection of odorant molecules and play a crucial role in the sense of smell.

Figure 1. Demonstration of Omni-DNA’s cross-modal capabilities. Given a DNA sequence, Omni-DNA could generate a natural language description for functional annotations.

Genomic Foundation Models (GFMs) (Nguyen et al., 2024; Zhou et al., 2023; Dalla-Torre et al., 2024; Schiff et al., 2024), a type of Deep Neural Networks (DNNs) for genomic sequence modeling, has emerged as essential tools to automate the annotation process. GFMs has been used for associating mutation in the genome with diseases (Benegas et al., 2023; Cheng et al., 2023), revealing regulatory effects of genomic sequences (Avsec et al., 2021a; Linder et al., 2025), and genomic elements annotation (de Almeida et al., 2024). Although these GFMs achieve great performance on genomic tasks (Zhou & Troyanskaya, 2015; Grešová et al., 2023), they are still far away from generalist models, which can handle multiple tasks simultaneously. This contrasts with Large Language Models (LLMs) (Radford et al., 2019; Team et al., 2023; Touvron et al., 2023), which have seen remarkable success at solving general tasks from question answering to theorem proofs (Xin et al., 2024). The success of LLMs is pretraining transformer-based auto-regressive models (Vaswani, 2017) on internet-scale data, followed by post-training to increase instruction-following abilities (Lambert et al., 2024). Inspired by this, we ask: *is it possible to develop a generalist genomic foundation model for addressing diverse genomic tasks simultaneously?*

Existing GFMs vary significantly in architecture and tokenization strategies, but they all follow a “pretrain + task-specific finetune” paradigm: first pretraining on unlabeled DNA sequences, and task-specific Multi-Layer Perceptrons

(MLPs) are attached for finetuning. This paradigm limits the generalization of the model in two ways. **(i)** The pretrained model needs to be separately finetuned K times given K tasks. This results in the additional cost of storing $\mathcal{O}(K)$ copies of model weights, incurring significant I/O latency, memory costs, and context-switching penalties. This also prevents models from leveraging shared biological patterns (e.g., conserved regulatory motifs or chromatin accessibility signatures (Van Roey et al., 2012; Yang et al., 2023)) across finetuning tasks. **(ii)** The output space of existing models is rigidly constrained to DNA sequences or pre-defined genomic labels, limiting their ability to generate diverse, semantically meaningful outputs. As a result, current GFMs struggle for multi-modal downstream tasks such as DNA2Text and DNA2Image.

To overcome these limitations, we introduce Omni-DNA, a family of cross-modal multi-task models ranging from 20 million to 1 billion parameters. This is achieved through carefully ablated pretraining of transformer-based auto-regressive models on DNA sequences and cross-modal multi-task finetuning.

The *pretraining* stage explores previously overlooked key configurations and their impact on training dynamics. This includes a comparison of non-parametric LayerNorm (Ba, 2016) vs. RMSNorm (Zhang & Sennrich, 2019), RoPE (Su et al., 2024) vs. ALiBi (Press et al., 2021) positional embeddings, and other configurations, ultimately leading Omni-DNA to achieve state-of-the-art performance on 18 out of 26 tasks on the Nucleotide Transformer (Dalla-Torre et al., 2024) and GB benchmarks (Grešová et al., 2023). When evaluated with a conventional paradigm, Omni-DNA outperforms existing bidirectional models.

Cross-modal multi-task finetuning expands the vocabulary in the model’s tokenizer by dynamically modifying the embedding matrix. To address the distribution shift of existing tokens due to vocabulary expansion (Hewitt, 2021), we propose *Important Key Repetition* and adopt NEFTune (Jain et al., 2023). Additionally, we implement a task unification strategy, aligning multiple genomic tasks under a unified format. The combination of these techniques enables a single model to solve multiple acetylation and methylation tasks at once, surpassing models trained on each task individually, as demonstrated in Figure 2. Furthermore, beyond conventional genomic tasks, Omni-DNA explores direct mapping from DNA sequences to functional descriptions and images, unlocking cross-modal capabilities.

In summary, our contributions are three-fold:

- (1) We revisit the auto-regressive transformers for GFMs, indicating the potential of next token prediction paradigm.
- (2) We present Omni-DNA, a unified cross-modal and multi-task GFM ranging from 20M to 1B parameters, achieving SOTA performance on multiple conventional benchmarks.

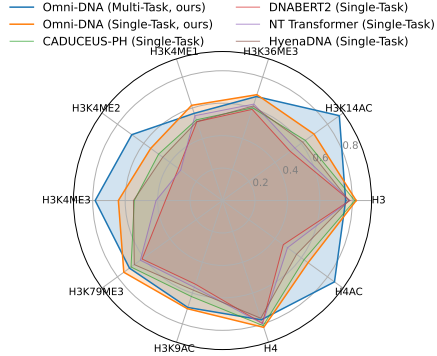


Figure 2. Accuracy comparison of Omni-DNA@mult. against Omni-DNA@sgl. and baselines across 10 NT tasks. Omni-DNA@mult. achieves the highest average accuracy.

- (3) We evaluate Omni-DNA on novel cross-modal and multi-task genomic tasks, such as DNA2Func and DNA2Image.

2. Preliminaries and Notations

2.1. Genomic Sequence Modeling

DNA is a polymer made of up four types of nucleotides: Adenine (A), Thymine (T), Guanine (G), and Cytosine (C). Let $\mathbb{N}_4 = \{A, T, G, C\}$. A DNA sequence of length T , denoted as $\mathbf{x} = (\mathbf{x}_1, \mathbf{x}_2, \dots, \mathbf{x}_T) \in \mathbb{N}_4^T$, follows a natural distribution $\mathbf{x} \sim p_\theta(\mathbf{x})$. We use $p_{\hat{\theta}}(\mathbf{x})$ to represent an estimate to the true distribution. The dataset of unlabeled genomic sequences is given in the form of $\{\mathbf{x}^{(i)}\}_{i=1}^N$.

Genomic sequence modeling aims to learn a function f that maps input sequences to biological annotations using a labeled dataset $\mathcal{D} = \{\mathbf{x}^{(i)}, \mathbf{y}^{(i)}\}_{i=1}^N$. The type of $y^{(i)}$ varies depending on the types of tasks: $y^{(i)}$ is a class label in **DNA Sequence Classification** (Grešová et al., 2023; Dalla-Torre et al., 2024). Or a real value vector in **Genomic Assay Prediction** tasks (Avsec et al., 2021a; Linder et al., 2025). Current genomic sequence models typically follow a two-stage strategy. In the pretraining phase, we learn the data distribution $p_{\hat{\theta}}(x)$ on a unlabeled dataset from unlabeled data using losses such as masked language modeling (MLM) $p(\mathbf{x}) = \prod_{t \in \mathcal{M}} p_\theta(\mathbf{x}_t | \mathbf{x}_{1:t-1}, \mathbf{x}_{t+1:T})$ or next token prediction (NTP) $p(\mathbf{x}) = \prod_{t=1}^T p_\theta(\mathbf{x}_t | \mathbf{x}_{1:t-1})$.

2.2. Supervised Finetuning

Supervised Finetuning (SFT) plays a key role in enhancing the instruction-following (Mishra et al., 2021; Sanh et al., 2021; Wei et al., 2022) and reasoning capabilities (Lambert et al., 2024). For a pretrained auto-regressive model with a fixed vocabulary V_x and a labeled dataset \mathcal{D} , SFT maximizes the likelihood: $\hat{\theta} = \arg \max_{\theta} \sum_{i=1}^N \log p_\theta(\mathbf{y}^{(i)} | \mathbf{x}^{(i)})$. This process retains the model’s pretrained knowledge while aligning its outputs with task-specific objectives, typically

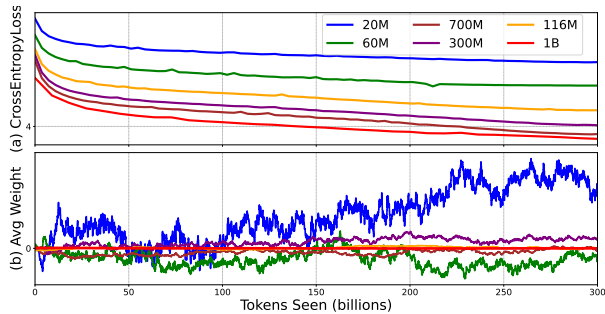


Figure 3. (a) **Cross Entropy Loss** on test set during pretraining. The models with varying sizes show a stable decrease in loss. (b) **No-Bias Normalization Layer** stabilizes the average value of feed-forward weights in transformer layers. This pattern is consistent across all the transformer blocks.

using **cross-entropy loss** on the target tokens:

$$p_{\theta}(\mathbf{y}^{(i)}|\mathbf{x}^{(i)}) = \sum_{i=1}^N \sum_{t=1}^{T'} \log p_{\theta}(\mathbf{y}_t^{(i)}|\mathbf{y}_{1:t-1}^{(i)}, \mathbf{x}^{(i)}). \quad (1)$$

Notably, \mathbf{y} could include new set of vocabulary V_z that do not overlap with V_o . Therefore, each term in Equation (1) is computed through Equation (2).

$$p_{\theta}(\mathbf{y}_t | \mathbf{y}_{1:t-1}, \mathbf{x}) = \frac{\exp(h_{t-1}^{\top} e_{\mathbf{y}_t})}{\sum_{m \in V_o} \exp(h_{t-1}^{\top} e_m) + \sum_{n \in V_z} \exp(h_{t-1}^{\top} e_n)}, \quad (2)$$

where h_{t-1} is the neural representation of the prefix sequence $(\mathbf{y}_{1:t-1}, \mathbf{x})$, e_m is the embedding of vocab m .

As a result, during the finetuning stage, the embeddings for each new vocabulary token $n \in V_z$ must be initialized, and the original token probabilities are shifted due to the expanded output space, as detailed in Hewitt (2021).

3. Approach

In this section, we introduce Omni-DNA with various model sizes for genomic tasks. The pretraining process is present in Section 3.1, followed by cross-modal multi-task finetuning in Section 3.2. The framework is illustrated in Figure 4.

3.1. Pretraining

Pretraining Dynamics: we pretrain a series of autoregressive transformer-based models using unlabeled DNA data, with log-uniformly spaced sizes ranging from 20 Million to 1 Billion. The pretraining procedure are conducted with minimum loss spike as shown in Figure 3(a) across models with various sizes. These model are trained on 300 billion nucleotides. The full hyperparameters used by our model and a comparison with prior genomic models are shown in Appendix A, below highlights key configurations.

Model Architecture: We build on Open Language Model (OLMo) (Groeneveld et al., 2024) for DNA Sequence Modeling. Compared to the vanilla transformer (Vaswani, 2017), several improvements introduced by LLaMA family (Touvron et al., 2023) and OLMo family are adopted to our model. (i) **LayerNorm** The Non-parametric layer norm (Ba, 2016) without Bias are applied to our 116M and 1B model. RMSNorm (Zhang & Sennrich, 2019) are applied to the remaining fours models. We find while both types of LayerNorm result in a stable pretraining process, the Non-parametric layer norm tends to maintain more stable average weights on the feed forward layer as shown in Figure 3, which in turns help to achieve higher accuracy when performing fullsize finetuning on the downstream tasks (Section 4). (ii) **Relative Positional Embeddings** Although previous work (Zhou et al., 2023) indicates that relative positional embedding methods such as ALiBi (Press et al., 2021) may offer improved extrapolation capabilities, the context length of the pretrained model can still be easily extended during finetuning. We observed slower convergence when using ALiBi in our pretraining experiments (see Section 6). (iii) **BPE Tokenizer** We adopt Byte-Pair Encoding (BPE) (Sennrich, 2015) with an initial vocabulary of 4096, following Zhou et al. (2023). During the vocabulary expansion, newly added tokens are always recognized as standalone tokens rather than retraining the tokenizer.

Pretraining Dataset Deduplication Duplicate data can slow model convergence, making deduplication standard in LLM pretraining (Rae et al., 2021; Groeneveld et al., 2024). Because genomic data is highly duplicated, we removed exact duplicates from NCBI’s multi-species genome dataset (Schoch et al., 2020), reducing it to 30 billion nucleotides. Despite this reduction, multiple epochs can still be used in training.

3.2. Cross-modal Multi-task Finetuning

Here we extend pretrained models to handle multiple modalities beyond DNA tokens and enable learning of diverse downstream tasks through a single finetuning process. We first introduce the whole process of finetuning and then describe the detailed modules.

Whole Process As illustrated in Algorithm 1, we need to finetune K task-specific datasets with different token sets and modalities. We first merge K task-specific datasets into a unified dataset \mathcal{D}_{uni} , and the tokenizer vocabulary are expanded to include unique new tokens from each task. During each training iteration, a batch of $(x^{(i)}, y^{(i)})_{i=1}^B$ is first sampled from \mathcal{D}_{uni} , $y^{(i)}$ is replicated by a factor α to emphasize class labels, and the loss is computed. The parameters θ are then updated via gradient-based optimization. By unifying multiple tasks under a single loop, the algorithm

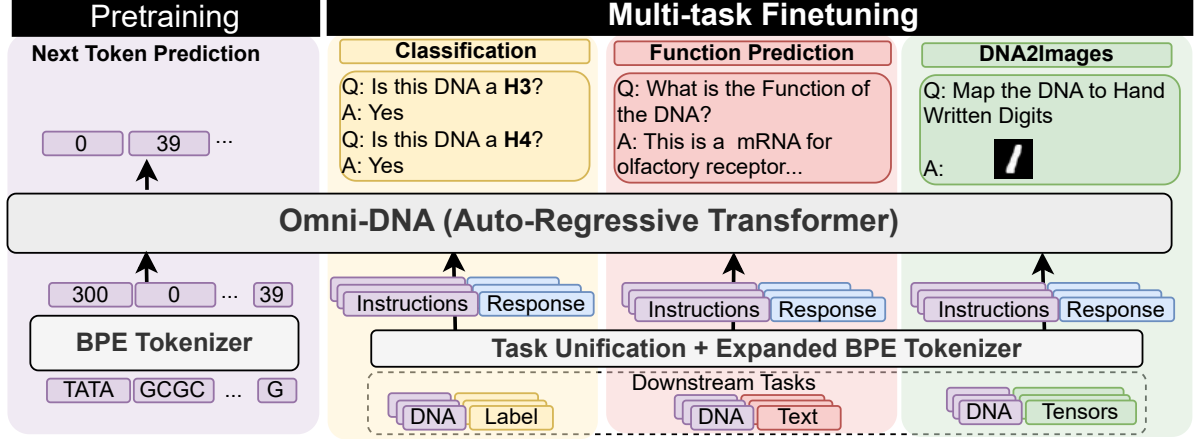


Figure 4. Overview of Omni-DNA architecture. In pretraining, Omni-DNA are trained on DNA only with next-token prediction. Multi-task finetuning enables the model to perform diverse tasks including classification, function prediction, and DNA-to-image.

Table 1. Examples of Genomic Task Unification, including inputs, labels, instructions, and responses.

Task Type	Original		Unified Format	
	Input $x^{(i)}$	Target $y^{(i)}$	Instruction $\tilde{x}^{(i)}$	Response $\tilde{y}^{(i)}$
Promoter CLS (2024)	AT...T	0/1	AT...Tis this a promoter?	Yes/No
Enhancer Types CLS (2024)	AT...A	0/1/2	AT...Awhat is enhancer type?	Type 0/1/2
DNA2Image	AT...G		AT...Gmap to image	[0, 2, ..., 512] (discretized tokens)
DNA2Text	AT...T	It encodes H-box helicase protein	AT...Twhat is the function?	It encodes H-box helicase protein

Algorithm 1 Cross-modal Multi-task Finetuning

Require: K datasets $\{\mathcal{D}_k\}_{k=1}^K$, pretrained model f_θ , vocabulary $V_{\text{pretrained}}$, repeating factor α , Noise Level β

- 1: $\mathcal{D}_{\text{uni}} \leftarrow \bigcup_{k=1}^K \mathcal{D}_k$ ▷ Task Unification
- 2: Extract task-specific multi-modal tokens V_k from \mathcal{D}_k
- 3: $V_{\text{expand}} \leftarrow V_{\text{pretrained}} \cup \bigcup_{k=1}^K V_k$ ▷ Vocab. expansion
- 4: **repeat**
- 5: $\{(x^{(i)}, y^{(i)})\}_{i=1}^B \sim \mathcal{D}_{\text{uni}}$ ▷ Batch size B
- 6: **for** i from 1 to B **do**
- 7: $y^{(i)} \leftarrow \text{ReplicateKeyToken}(y^{(i)}, \alpha)$ ▷ Replicate Class Labels in target for Classification Tasks
- 8: $\text{loss}^{(i)} \leftarrow -\sum_{t=1}^{|y^{(i)}|} \log p_\theta(y_t^{(i)} | y_{1:t-1}^{(i)}, x^{(i)}, \beta)$ ▷ Add noise using NEFTune with β during loss computing
- 9: **end for**
- 10: $\text{Loss}_{\text{batch}} \leftarrow \frac{1}{B} \sum_{i=1}^B \text{loss}^{(i)}$
- 11: $\theta \leftarrow \text{optimizer}(\theta, \text{Loss}_{\text{batch}})$
- 12: **until** stopping criterion or max iterations

encourages the model improves the average performance across diverse genomic tasks.

Multi-task Dataset Unification We integrate K genomic tasks with labeled datasets $\{\mathcal{D}_k\}_{k=1}^K$ of various formats into a unified dataset $\mathcal{D}_{\text{uni}} = \{\tilde{x}^{(i)}, \tilde{y}^{(i)}\}$. Specifically, each sample from task k is modified by appending a task-specific prompt Prompt_k to its input $x^{(i)}$: $\tilde{x}^{(i)} = (x^{(i)}, \text{Prompt}_k)$. The corresponding response $\tilde{y}^{(i)}$ is treated as tokens and the

typical transformation is shown in Table 1.

Vocabulary Expansion As the multi-task dataset unification introduces new tokens (i.e., prompt and response tokens), it is necessary to expand the vocabulary during SFT stage. This is a key difference between genomic language model and normal language models. A direct result of vocabulary expansion is distribution shift. Based on (Hewitt, 2021), the distribution shift after adding a new set of vocabulary V_z to pretrained model θ results in a new model θ' , let $Z = \sum_{m \in V_o} \exp(h_{t-1}^T e_m)$. Then the distribution shift are:

$$p_{\theta'}(x_t | x_{1:t-1}) = p_\theta(x_t | x_{1:t-1}) \cdot \frac{1}{1 + \frac{\sum_{n \in V_z} \exp(h_{t-1}^T e_n)}{Z}}. \quad (3)$$

In other words, all the words probability are reduced. To alleviate it, we should minimize the size of added tokens.

NEFTune & Key Token Replication To mitigate catastrophic forgetting (Zheng et al., 2024) caused by distribution shifts from vocabulary expansion, we employ two simple yet effective techniques: *NEFTune* (Press et al., 2021) and *Key Token Replication*. NEFTune introduces random noise to embedding vectors during finetuning, reducing overfitting. Key Token Replication, applied to classification tasks, replicates label tokens in $y^{(i)}$ by a factor of α . This ensures stronger signal propagation, facilitating the model’s tran-

sition from DNA sequence generation to classification by reinforcing the association between input sequences and their corresponding labels.

Response Discretization In many genomic tasks such as genomic assay prediction (Avsec et al., 2021a) and structure prediction (Abramson et al., 2024), the response is a high-dimensional continuous variable $\mathbf{y} \in \mathbb{R}^{d_1 \times d_2 \times \dots \times d_k}$. To adopt Omni-DNA, we need to discretize the response first.

Here we consider a three-dimensional continuous variable $\mathbf{y} \in \mathbb{R}^{d_1 \times d_2 \times d_3}$. *Response discretization* is achieved by training a VQ-VAE (Van Den Oord et al., 2017), which learns a latent embedding space of dimension $[K, D]$, where K represents the number of quantized embeddings, and D denotes the dimensionality of each latent embedding vector $\mathbf{e}_i \in \mathbb{R}^D$. The VQ-VAE compresses the input $\mathbf{y}^{(i)}$ to a sequence of discrete latent variables $\tilde{\mathbf{y}}^{(i)} = \{e_0, e_1, \dots, e_L\} \in \mathbb{N}_K^L$. Here, $L = d'_1 \times d'_2$ corresponds to the spatial dimensions of the encoded variable $\tilde{\mathbf{y}}^{(i)}$, where $d'_1 = d_1/r$ and $d'_2 = d_2/r$. The compression ratio r quantifies the reduction in dimensionality achieved during encoding. The decoder then reconstructs the input \mathbf{y} from discrete latent sequences $\tilde{\mathbf{y}}$. By employing response discretization, any DNA-to-continuous-variable task can be converted into a DNA-to-discrete-token task.

4. Results on Conventional Genomics Tasks

Setup To evaluate the quality of Omni-DNA and establish a baseline for multi-tasking, we first follow the conventional evaluation process in single task mode. We compare Omni-DNA with DNABERT-2 (Zhou et al., 2023), NT-Transformer (Dalla-Torre et al., 2024), HyenaDNA (Nguyen et al., 2024), and Caduceus models (Schiff et al., 2024), across two widely used benchmarks: NT-Downstream Tasks (Dalla-Torre et al., 2024) and Genomic Benchmark (Grešová et al., 2023). Evaluation is performed using a conventional approach, where a MLP head is attached to the pretrained models, followed by full-size finetuning. The detailed set up of the evaluation is in Appendix D.

4.1. Nucleotide Transformer Downstream Tasks

NT Downstream Tasks include 18 distinct binary or three-class classification tasks. These tasks can be categorized into four categories: epigenetic marker (Pokholok et al., 2005), promoter (Oubounyt et al., 2019), enhancer and splice site prediction. Following the prior evaluation setup (Schiff et al., 2024), Matthews Correlation Coefficient (MCC) is used for histone marker and enhancer, while F1-score is used for splice and promoter classification. We finetune each model with 10-fold cross-validation (Schiff et al., 2024), with maximum epochs set to 20.

Table 2 shows the average performance of 16 models across different tasks types and the average performance across 18 tasks. Omni-DNA (1B) and Omni-DNA (116M) achieve the best average performance of 0.767 and the second of 0.755. Both models are trained with non-parametric norm. We provide the task-specific performance of 16 models in Table 8, Omni-DNA achieves superior performance on 13 out of 18 benchmark tasks, surpassing competing methods. Task-specific results in Table 8 show that Omni-DNA outperforms competing methods on 13 out of 18 benchmarks. For the remaining five tasks, Omni-DNA (1B) ranks second and third in Promoter:ALL and Promoter:NonTATA. In the three splice site classification tasks, Omni-DNA models perform lower than NT models but still surpass other models.

4.2. Genomic Benchmark Results

Genomic Benchmark (GB) (Grešová et al., 2023) contains eight DNA regulatory element classification tasks, similar to NT downstream tasks, with additional tasks on species classification and gene regulatory element classification on mouse. The number of sequences from seven tasks in GB was 10 times larger compared to NT downstream tasks. The details on the finetuning setting are included in Appendix D. Each model was finetuned for a max of 10 epochs. We compare the performance of smaller size model from each type of the model in Table 3.

Omni-DNA (116M) achieved the highest average score, ranking first in five out of eight tasks and second in the remaining three. Compared to DNABERT-2, which has a similar model size, Omni-DNA (116M) outperformed DNABERT-2 in seven out of eight tasks.

5. Building Cross-modal Multi-task Genomic Foundation Models

In this section, we demonstrate the **cross-modal multi-task** capability of Omni-DNA in using DNA sequences to three distinct modalities: discrete labels, textual descriptions, and images. The first two are derived from real-world datasets, while the third is based on a synthetic dataset called *Needle-in-DNA*. Despite the significant differences in task formats, a unified approach is employed to address all three.

For classification problems, Omni-DNA finetuned with multiple tasks not only has the ability to solve more than one task simultaneously but also improves overall model performance on related NT downstream tasks: a phenomenon we refer to as the **synergistic effect**. Additionally, we extend beyond conventional genomic modeling tasks to tackle more challenging and general problems: (1) DNA-to-function and (2) DNA-to-image. These efforts underscore the potential of training a unified genomic foundation model capable of acting as a generalist across both tasks and modalities.

Table 2. Comparison of Omni-DNA with existing GFMs on 18 NT downstream tasks. The family of Omni-DNA obtains the best average result. In splice tasks, Omni-DNA performs lower than NT models but still surpasses other models.

Pretraining Objective	Pretraining Data	Model	Histone (AVG. MCC in 10 Tasks) \uparrow	Enhancer (AVG. MCC in 2 Tasks) \uparrow	Promoter (AVG. F1 in 3 Tasks) \uparrow	Splice (AVG. F1 in 3 Tasks) \uparrow	Average (Across 18 Tasks) \uparrow
MLM	Human	CADUCEUS-PH (1.9M)	0.635	0.4925	0.964	0.942	0.715
		CADUCEUS-PS (1.9M)	0.585	0.454	0.964	0.912	0.689
	Multi-Species	DNABERT2 (120M)	0.551	0.470	0.966	0.959	0.679
		NT (50M)	0.493	0.465	0.953	0.980	0.648
		NT (100M)	0.496	0.475	0.957	0.983	0.661
		NT (250M)	0.536	0.472	0.968	0.983	0.675
		NT (500M)	0.572	0.486	0.972	0.983	0.698
NT (2.5B)	0.584	0.527	0.971	0.986	0.709		
NTP	Human	HyenaDNA (1.6M)	0.610	0.452	0.954	0.954	0.707
	Multi-Species (Ours)	Omni-DNA (20M)	0.538	0.484	0.957	0.897	0.662
		Omni-DNA (60M)	0.559	0.499	0.966	0.938	0.690
		Omni-DNA (116M)	0.675	0.545	0.970	0.960	0.755
		Omni-DNA (300M)	0.659	0.486	0.969	0.956	0.741
		Omni-DNA (700M)	0.675	0.519	0.968	0.960	0.754
		Omni-DNA (1B)	0.694	0.536	0.973	0.958	0.767

Table 3. Performance of Omni-DNA across 8 tasks in the genomic benchmark. Omni-DNA (116M) achieves the highest average. \pm indicates the difference between the max and min value in 10 fold cross-validation.

Task Name	CNN (264K)	HYENADNA (436K)	CADUCEUS -PH (470K)	DNABERT2 (117M)	Omni-DNA (116M)
MOUSE ENHANCERS	0.715 \pm 0.087	0.780 \pm 0.025	0.754 \pm 0.074	0.792 \pm 0.031	0.799 \pm 0.004
CODING VS. INTERGENOMIC	0.892 \pm 0.008	0.904 \pm 0.005	0.915 \pm 0.003	0.949 \pm 0.002	0.942 \pm 0.010
HUMAN VS. WORM	0.942 \pm 0.002	0.964 \pm 0.002	0.973 \pm 0.001	0.975 \pm 0.002	0.976 \pm 0.001
HUMAN ENHANCERS COHN	0.702 \pm 0.021	0.729 \pm 0.014	0.747 \pm 0.004	0.714 \pm 0.025	0.738 \pm 0.002
HUMAN ENHANCER ENSEMBL	0.744 \pm 0.122	0.849 \pm 0.006	0.893 \pm 0.008	0.891 \pm 0.051	0.919 \pm 0.021
HUMAN REGULATORY	0.872 \pm 0.005	0.869 \pm 0.012	0.872 \pm 0.011	0.852 \pm 0.024	0.895 \pm 0.012
HUMAN OCR ENSEMBL	0.698 \pm 0.013	0.783 \pm 0.007	0.828 \pm 0.006	0.789 \pm 0.012	0.791 \pm 0.001
HUMAN NONTATA PROMOTERS	0.861 \pm 0.009	0.944 \pm 0.002	0.946 \pm 0.007	0.912 \pm 0.013	0.968 \pm 0.013
Average	0.803	0.853	0.866	0.859	0.879

5.1. Multi-Task Model for Acetylation and Methylation

Task In the NT downstream tasks, 10 related tasks—H3, H3K14AC, H3K36ME3, H3K4ME1, H3K4ME2, H3K4ME3, H3K79ME3, H3K9AC, H4, and H4AC—are considered. These tasks are interconnected due to the biological correlation between acetylation and methylation effects (Pokholok et al., 2005). The objective here is to train a model capable of addressing all 10 tasks with a single fine-tuning step. While conventional fine-tuning approaches with a classification head struggle to address this challenge, *cross-modal multi-task finetuning* unifies these tasks into a single model. At inference time, having an omni-model that solves all tasks eliminates the need for context switching and repeated fine-tuning.

We use Omni-DNA (1B) to complete 10 acetylation and methylation tasks using multi-task finetuning with NEF-Tune noise level = 5 and repeating factor = 10. The baselines include the best-performing single-task models: Omni-

DNA (1B) and CADUCEUS-PH (1.9M), as presented in Section 4, along with DNABERT-2 and NT (500M) as references. Conventionally, multi-task finetuning may lead to performance drop compared with single-task finetuning due to the challenge of balancing generalizability across tasks. However, by grouping similar tasks, we observe significant improvements. The results, shown in Table 4 and Figure 2, demonstrate that Omni-DNA@mult achieves dramatic improvements in 4 tasks, and obtains the highest average accuracy. This indicates that the resulting model not only reduces the burden of context switching and repetitive finetuning but also leverages the internal relationships between tasks to achieve higher performance than its single-task counterparts. We refer to this phenomenon as the **synergistic effect**, which emerges in finetuning genomic foundation models in a multi-task setting.

Table 4. Performance comparison across 10 related acetylation and methylation tasks. Omni-DNA@mult. outperforms single-task models in 4 tasks, and achieves the second-best performance in 5 tasks, demonstrating the synergistic effect of multi-task genomic fine-tuning.

	Omni-DNA@mult. (1B)	Omni-DNA@sgl. (1B)	DNABERT2@sgl. (117M)	NT Transformer@sgl. (500M)	CADUCEUS-PH@sgl. (1.9M)
H3	0.759 ± 0.021	0.824 ± 0.032	0.785 ± 0.033	0.784 ± 0.047	0.815 ± 0.048
H3K14AC	0.890 ± 0.011	0.697 ± 0.077	0.516 ± 0.028	0.551 ± 0.021	0.631 ± 0.026
H3K36ME3	0.674 ± 0.008	0.686 ± 0.002	0.591 ± 0.020	0.625 ± 0.013	0.601 ± 0.129
H3K4ME1	0.565 ± 0.015	0.617 ± 0.000	0.511 ± 0.028	0.550 ± 0.021	0.523 ± 0.039
H3K4ME2	0.691 ± 0.008	0.547 ± 0.006	0.336 ± 0.040	0.319 ± 0.045	0.487 ± 0.170
H3K4ME3	0.785 ± 0.008	0.642 ± 0.001	0.352 ± 0.077	0.410 ± 0.033	0.544 ± 0.045
H3K79ME3	0.709 ± 0.017	0.752 ± 0.007	0.613 ± 0.030	0.626 ± 0.026	0.697 ± 0.077
H3K9AC	0.693 ± 0.013	0.701 ± 0.002	0.542 ± 0.029	0.562 ± 0.040	0.622 ± 0.030
H4	0.773 ± 0.013	0.822 ± 0.005	0.796 ± 0.027	0.799 ± 0.025	0.811 ± 0.022
H4AC	0.853 ± 0.014	0.652 ± 0.001	0.463 ± 0.041	0.495 ± 0.032	0.621 ± 0.054
Average	0.739	0.694	0.551	0.572	0.635

5.2. Functional Annotation Generation (DNA2Func)

Dataset and Task As shown in Figure 10, we have constructed a large-scale DNA sequence dataset enriched with text-based functional annotations. This dataset comprises 330,000 sequences from various mammalian species, and each sequence is annotated with a concise short annotation followed by a more detailed natural language description. We split the dataset into finetuning and test sets with a 9:1 ratio. The full workflow for dataset construction is in Appendix F. This is a multi-task scenario with two objectives: (1) generating concise short annotations for DNA sequences and (2) further explaining the corresponding functions by natural language.

Baselines We finetuned our proposed Omni-DNA, using the finetuning dataset, denoted as Omni-DNA@ft. Since conventional genomic foundation models cannot handle these tasks, we employed GPT-4o (GPT4o@zeroshot) to directly predict DNA functions using the prompt in Table 11. In addition, we included OLMo-1B as a baseline, a similar architecture model pre-trained on natural language, and finetuned on the same finetuning dataset with Omni-DNA, referred to as OLMo-1B@ft.

Evaluation & Metrics To evaluate the accuracy of free-form text is challenging. Thus, we leveraged an LLM (GPT4o) to judge whether the generated text and ground-truth are matched. We first utilized GPT4o to classify the generated text into seven function labels, as shown in Figure 10. Then the F1 scores and Matthews Correlation Coefficient (MCC) are computed between the classified labels and ground-truth.

Quantitative Results As shown in Table 5, Omni-DNA obtains the best result compared to GPT4o and OLMo-1B, highlighting the potential for solving this domain-specific

Table 5. Comparison of Weighted F1 Score and MCC for Omni-DNA@ft, GPT4o@zeroshot, OLMo-1B@ft, and Random Guess.

	Omni-DNA	GPT4o	OLMo-1B	Random
F1 Score	0.730	0.659	0.701	0.483
MCC	0.367	-0.015	0.342	0.008

problem. Tables 12 to 14 present representative responses from the three models. Among them, Omni-DNA@ft consistently demonstrates the strongest performance. In contrast, GPT4o fails to understand the meaning of the DNA sequences in all three examples, whereas the other two models provide more meaningful responses. Notably, Omni-DNA is capable of producing grammatical and novel sentences, rather than merely reproducing finetuning datasets.

5.3. Needle-in-DNA Task (DNA2Image)

Dataset and Task The identification of short functional motifs in DNA is pivotal for understanding gene regulation because these conserved subsequences often serve as transcription factor binding sites or other key regulatory elements (Tompa et al., 2005; Avsec et al., 2021b). Over the past decade, deep learning methods have further advanced motif discovery by more accurately predicting sequence specificities of DNA- and RNA-binding proteins (Alipanahi et al., 2015), thus refining our ability to pinpoint critical regulatory regions within the genome. Leveraging motif-aware learning for training LLMs, has proven effective for uncovering regulatory and structural elements in genomic sequences (Wang et al., 2024; Sanabria et al., 2024). Motivated by this, we generate a dataset consisting of 48,000 synthetic DNA sequences by a Hidden Markov Model. Each sequence contains one of four functional motifs (referred to as “needles”): {TATAAA, CAAT, GGGCGG, TTAGGG}, and is labeled 0, 1, 2, or 3 accordingly. Notably, the label is represented by an image of a handwritten digit {0, 1, 2, 3}.



Figure 5. F1 scores and invalid percentages for *Needle-in-DNA*, averaged and per class. Omni-DNA outperforms both baselines.

}, sampled from the MNIST dataset (Yadav & Bottou, 2019). The dataset is split into finetuning, validation, and test sets in an 8:1:1 ratio.

Following data discretization in Section 3.2, we train a VQ-VAE (Van Den Oord et al., 2017) with six quantized vectors of dimension 32 and a compression ratio of 4. This model converts the grayscale images of size 28×28 into 49 discrete tokens. It leverages a multi-task setting with two tasks: (1) classify the DNA sequences, and (2) generate the corresponding handwritten digit image. The details of dataset construction can be found in Appendix E.

Evaluation and Baselines To assess the benefit of pre-training on DNA sequences, we employ two baselines: OLMo-1B, a natural language model pretrained on text with instruction tuning, and the Vanilla Model, which shares Omni-DNA’s architecture but is randomly initialized without pretraining. The baselines and Omni-DNA (1B) are all fine-tuned on the fine-tuning dataset for 10 epochs.

The evaluation is conducted by two human annotators who independently assess the images generated by the three models. They provide two labels: (1) validity indicating whether the image represents a number from $\{0,1,2,3\}$, and (2) the corresponding digit if valid. Inconsistent answers between annotators are discarded. This labeling process identifies two types of errors: vague or non-meaningful images, and incorrect classification. Thus, two metrics are used to measure model performance: (1) **invalid percentage**, the proportion of generated images that are non-numeric or not in $\{0,1,2,3\}$, and (2) **macro F1 scores**, averaged across all valid samples, for each class.

Results Figure 5 shows that Omni-DNA achieves a Macro F1 score of 0.987 and an invalid percentage of 1% on average, significantly outperforming baselines. This indicates that Omni-DNA nearly solves the task perfectly. In contrast,

while OLMo-1B has a high F1 score in the motifs TATAAA (class 0) and CAAT (class 1), it struggles with GGGCGG (class 2) and TTAGGG (class 3). Since its invalid percentages are similar across these classes, the primary issue is generating incorrect digit images, indicating that OLMo-1B fails to classify DNA sequences accurately.

Beyond Memorization Our visualization results demonstrate that Omni-DNA does not merely memorize the fine-tuned images, but actually generates novel handwritten digits with various shapes. We verify that these examples are not present in the fine-tuning set, indicating that the model learns general digit patterns in $\{0,1,2,3\}$ conceptually rather than memorizing discretized tokens. See Figure 9 for generated examples.

6. Ablation Study

6.1. Ablation on Positional Embedding Methods

We utilized Omni-DNA (116M) to test the effect of two positional embedding methods: ALiBi (Press et al., 2021) and RoPE (Su et al., 2024). We perform pretraining on 300 billion nucleotides with keeping the remaining hyperparameters unchanged. The training and test losses during pretraining are shown in Figure 6. RoPE achieves a lower test loss and converges faster, indicating that it better captures the contextual and relational properties of DNA compared to ALiBi.

6.2. Larger Models Mitigate Distribution Shifts

Equation (3) shows that introducing new vocabulary leads to a distribution shift of existing tokens. While synergistic effects in multi-task settings can mitigate this shift (Son et al., 2024), single-task scenarios experience performance degradation when new tokens are added compared to using a classification head. Figure 7 shows how performance

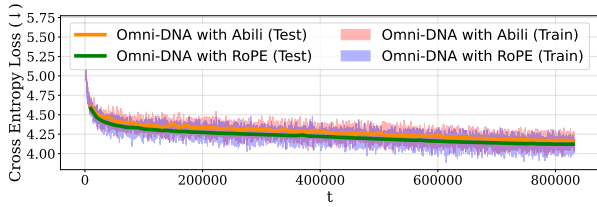


Figure 6. Losses for Omni-DNA (116M) pretrained with ALiBi and RoPE, indicating RoPE’s faster convergence and lower losses.

degradation varies with model size in the promoter TATA classification task. Notably, increasing the model size alleviates this issue, and Omni-DNA (1B) maintains performance comparable to those, prior to vocabulary expansion.

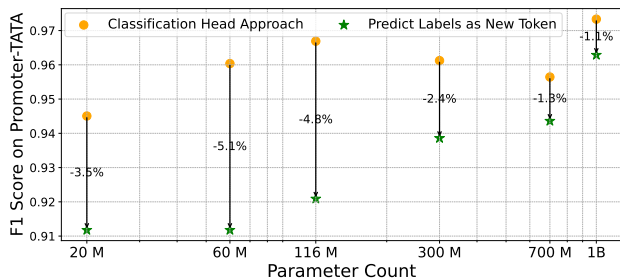


Figure 7. Impact of model size on performance degradation due to vocabulary expansion. Larger models exhibit better resilience against distribution shifts.

6.3. Impact of Token Replication Factor

Figure 8 illustrates the effect of the token replication factor α on the promoter TATA classification task for Omni-DNA sized 116M and 1B. Without token replication ($\alpha = 1$), classification performance is poor. We find that setting α within the range [8, 11] is effective across various task types.

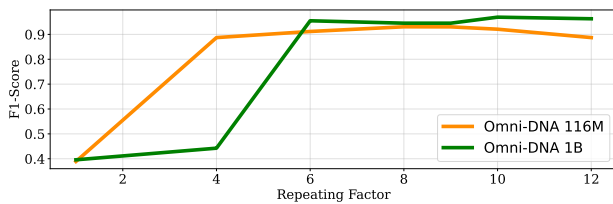


Figure 8. Impact of the token replication factor α on the promoter TATA classification task.

7. Conclusion

We have demonstrated that pretraining an auto-regressive transformer on DNA sequences, followed by cross-modal multi-task finetuning, is an effective strategy for constructing a unified genomic foundation model. This model can

handle diverse genomic tasks across multiple modalities, including discrete labels, textual descriptions, and other multi-dimensional outputs. Specifically, we demonstrate that: (i) The auto-regressive model can match or outperform the bidirectional transformer on genomic sequence modeling. (ii) The model pretrained solely on genomic sequences can generalize to unseen tokens through finetuning, achieving the SOTA performance. Our proposed Omni-DNA not only handles multiple classification tasks within a single model, but also tackles more complex challenges, such as converting DNA into coherent, contextually relevant natural language, and mapping DNA to multi-dimensional representations, as showcased in DNA2Funtion and DNA2image.

We hope that this paper with available codes for pretraining and finetuning, will serve as a starting point for researchers to explore more complex genomic tasks and develop more comprehensive genomics foundation models.

Limitations Our work primarily focuses on transformer-based architectures, leaving the exploration of alternative approaches, such as state-space models like Mamba (Gu & Dao, 2023) and Hyena (Nguyen et al., 2024), and recurrent neural network architectures like xLSTM (Schmidinger et al., 2024) for future research. Additionally, while our model demonstrates the feasibility of mapping DNA to multi-dimensional outputs, such as structure or genomic assay signals, achieving high-fidelity cross-modality translation remains an open challenge. Future improvements in tokenization strategies (Li et al., 2024a; Pagnoni et al., 2024; Qiao et al., 2024), including more robust vector quantization (VQ-VAE) techniques, could potentially improve the model’s ability to handle complex modalities with greater precision. Moreover, the DNA pretraining corpus, while extensive at 300B nucleotides, may not fully capture the diversity of regulatory elements across all species and tissue types (Andrews et al., 2023). Finally, while we have demonstrated strong performance on regulatory element classification and selected tasks, our evaluation does not encompass important genomic challenges like long-range interaction prediction (Cheng et al., 2025) or variant effect prediction (Li et al., 2024b).

References

Abramson, J., Adler, J., Dunger, J., Evans, R., Green, T., Pritzel, A., Ronneberger, O., Willmore, L., Ballard, A. J., Bambrick, J., et al. Accurate structure prediction of biomolecular interactions with alphafold 3. *Nature*, pp. 1–3, 2024.

Alipanahi, B., DeLong, A., Weirauch, M. T., and Frey, B. J. Predicting the sequence specificities of dna-and rna-binding proteins by deep learning. *Nature Biotechnology*, 33(8):831–838, 2015.

- Andrews, G., Fan, K., Pratt, H. E., Phalke, N., §, Z. C., Karlsson, E. K., Lindblad-Toh, K., Gazal, S., Moore, J. E., Weng, Z., et al. Mammalian evolution of human cis-regulatory elements and transcription factor binding sites. *Science*, 380(6643):eabn7930, 2023.
- Avsec, Ž., Agarwal, V., Visentin, D., Ledsam, J. R., Grabska-Barwinska, A., Taylor, K. R., Assael, Y., Jumper, J., Kohli, P., and Kelley, D. R. Effective gene expression prediction from sequence by integrating long-range interactions. *Nature methods*, 18(10):1196–1203, 2021a.
- Avsec, Ž., Weilert, M., Shrikumar, A., Krueger, S., Alexandari, A., Dalal, K., Fropf, R., McAnany, C., Gagneur, J., Kundaje, A., et al. Base-resolution models of transcription-factor binding reveal soft motif syntax. *Nature genetics*, 53(3):354–366, 2021b.
- Ba, J. L. Layer normalization. *arXiv preprint arXiv:1607.06450*, 2016.
- Benegas, G., Batra, S. S., and Song, Y. S. Dna language models are powerful predictors of genome-wide variant effects. *Proceedings of the National Academy of Sciences*, 120(44):e2311219120, 2023.
- Cheng, J., Novati, G., Pan, J., Bycroft, C., Žemgulytė, A., Applebaum, T., Pritzel, A., Wong, L. H., Zielinski, M., Sargeant, T., et al. Accurate proteome-wide missense variant effect prediction with alphamissense. *Science*, 381(6664):eadg7492, 2023.
- Cheng, W., Song, Z., Zhang, Y., Wang, S., Wang, D., Yang, M., Li, L., and Ma, J. Dnalongbench: A benchmark suite for long-range dna prediction tasks. *bioRxiv*, pp. 2025–01, 2025.
- Dalla-Torre, H., Gonzalez, L., Mendoza-Revilla, J., Lopez Carranza, N., Grzywaczewski, A. H., Oteri, F., Dallago, C., Trop, E., de Almeida, B. P., Sirelkhatim, H., et al. Nucleotide transformer: building and evaluating robust foundation models for human genomics. *Nature Methods*, pp. 1–11, 2024.
- de Almeida, B. P., Dalla-Torre, H., Richard, G., Blum, C., Hexemer, L., Gélard, M., Mendoza-Revilla, J., Pandey, P., Laurent, S., Lopez, M., et al. Segmentnt: annotating the genome at single-nucleotide resolution with dna foundation models. *bioRxiv*, pp. 2024–03, 2024.
- Grešová, K., Martinek, V., Čechák, D., Šimeček, P., and Alexiou, P. Genomic benchmarks: a collection of datasets for genomic sequence classification. *BMC Genomic Data*, 24(1):25, 2023.
- Groeneveld, D., Beltagy, I., Walsh, P., Bhagia, A., Kinney, R., Tafjord, O., Jha, A. H., Ivison, H., Magnusson, I., Wang, Y., et al. Olmo: Accelerating the science of language models. *arXiv preprint arXiv:2402.00838*, 2024.
- Gu, A. and Dao, T. Mamba: Linear-time sequence modeling with selective state spaces. *arXiv preprint arXiv:2312.00752*, 2023.
- Hewitt, J. Initializing new word embeddings for pre-trained language models. URL: <https://nlp.stanford.edu/~johnhew/vocab-expansion.html>, 2021.
- Jain, N., Chiang, P.-y., Wen, Y., Kirchenbauer, J., Chu, H.-M., Somepalli, G., Bartoldson, B. R., Kailkhura, B., Schwarzschild, A., Saha, A., et al. Neftune: Noisy embeddings improve instruction finetuning. *arXiv preprint arXiv:2310.05914*, 2023.
- Lambert, N., Morrison, J., Pyatkin, V., Huang, S., Ivison, H., Brahman, F., Miranda, L. J. V., Liu, A., Dziri, N., Lyu, S., et al. T”ulu 3: Pushing frontiers in open language model post-training. *arXiv preprint arXiv:2411.15124*, 2024.
- Lathe, W., Williams, J., Mangan, M., and Karolchik, D. Genomic data resources: challenges and promises. *Nature Education*, 1(3):2, 2008.
- Li, S., Wang, Z., Liu, Z., Wu, D., Tan, C., Zheng, J., Huang, Y., and Li, S. Z. Vqdna: Unleashing the power of vector quantization for multi-species genomic sequence modeling. *arXiv preprint arXiv:2405.10812*, 2024a.
- Li, Z., Subasri, V., Stan, G.-B., Zhao, Y., and Wang, B. Gv-rep: A large-scale dataset for genetic variant representation learning. *arXiv preprint arXiv:2407.16940*, 2024b.
- Linder, J., Srivastava, D., Yuan, H., Agarwal, V., and Kelley, D. R. Predicting rna-seq coverage from dna sequence as a unifying model of gene regulation. *Nature Genetics*, pp. 1–13, 2025.
- Mishra, S., Khashabi, D., Baral, C., Choi, Y., and Hajishirzi, H. Reframing instructional prompts to gptk’s language. *arXiv preprint arXiv:2109.07830*, 2021.
- Nguyen, E., Poli, M., Faizi, M., Thomas, A., Wornow, M., Birch-Sykes, C., Massaroli, S., Patel, A., Rabideau, C., Bengio, Y., et al. Hyenadna: Long-range genomic sequence modeling at single nucleotide resolution. *Advances in neural information processing systems*, 36, 2024.
- Oubounyt, M., Louadi, Z., Tayara, H., and Chong, K. T. Deepromoter: robust promoter predictor using deep learning. *Frontiers in genetics*, 10:286, 2019.
- Pagnoni, A., Pasunuru, R., Rodriguez, P., Nguyen, J., Muller, B., Li, M., Zhou, C., Yu, L., Weston, J., Zettlemoyer, L., et al. Byte latent transformer: Patches scale better than tokens. *arXiv preprint arXiv:2412.09871*, 2024.

- Pokholok, D. K., Harbison, C. T., Levine, S., Cole, M., Hannett, N. M., Lee, T. I., Bell, G. W., Walker, K., Rolfe, P. A., Herbolsheimer, E., et al. Genome-wide map of nucleosome acetylation and methylation in yeast. *Cell*, 122(4):517–527, 2005.
- Press, O., Smith, N. A., and Lewis, M. Train short, test long: Attention with linear biases enables input length extrapolation. *arXiv preprint arXiv:2108.12409*, 2021.
- Qiao, L., Ye, P., Ren, Y., Bai, W., Liang, C., Ma, X., Dong, N., and Ouyang, W. Model decides how to tokenize: Adaptive dna sequence tokenization with mxdna. *arXiv preprint arXiv:2412.13716*, 2024.
- Radford, A., Wu, J., Child, R., Luan, D., Amodei, D., Sutskever, I., et al. Language models are unsupervised multitask learners. *OpenAI blog*, 1(8):9, 2019.
- Rae, J. W., Borgeaud, S., Cai, T., Millican, K., Hoffmann, J., Song, F., Aslanides, J., Henderson, S., Ring, R., Young, S., et al. Scaling language models: Methods, analysis & insights from training gopher. *arXiv preprint arXiv:2112.11446*, 2021.
- Sanabria, M., Hirsch, J., Joubert, P. M., and Poetsch, A. R. Dna language model grover learns sequence context in the human genome. *Nature Machine Intelligence*, 6(8): 911–923, 2024.
- Sanh, V., Webson, A., Raffel, C., Bach, S. H., Sutawika, L., Alyafeai, Z., Chaffin, A., Stiegler, A., Scao, T. L., Raja, A., et al. Multitask prompted training enables zero-shot task generalization. *arXiv preprint arXiv:2110.08207*, 2021.
- Schiff, Y., Kao, C.-H., Gokaslan, A., Dao, T., Gu, A., and Kuleshov, V. Caduceus: Bi-directional equivariant long-range dna sequence modeling. *arXiv preprint arXiv:2403.03234*, 2024.
- Schmidinger, N., Schneckenreiter, L., Seidl, P., Schimunek, J., Hoedt, P.-J., Brandstetter, J., Mayr, A., Luukkonen, S., Hochreiter, S., and Klambauer, G. Bio-xlstm: Generative modeling, representation and in-context learning of biological and chemical sequences. *arXiv preprint arXiv:2411.04165*, 2024.
- Schoch, C. L., Ciufo, S., Domrachev, M., Hotton, C. L., Kannan, S., Khovanskaya, R., Leipe, D., Mcveigh, R., O’Neill, K., Robbertse, B., et al. Ncbi taxonomy: a comprehensive update on curation, resources and tools. *Database*, 2020:baaa062, 2020.
- Sennrich, R. Neural machine translation of rare words with subword units. *arXiv preprint arXiv:1508.07909*, 2015.
- Son, G., Baek, S., Nam, S., Jeong, I., and Kim, S. Multi-task inference: Can large language models follow multiple instructions at once? *arXiv preprint arXiv:2402.11597*, 2024.
- Su, J., Ahmed, M., Lu, Y., Pan, S., Bo, W., and Liu, Y. Roformer: Enhanced transformer with rotary position embedding. *Neurocomputing*, 568:127063, 2024.
- Team, G., Anil, R., Borgeaud, S., Alayrac, J.-B., Yu, J., Soricut, R., Schalkwyk, J., Dai, A. M., Hauth, A., Millican, K., et al. Gemini: a family of highly capable multimodal models. *arXiv preprint arXiv:2312.11805*, 2023.
- Tompa, M., Li, N., Bailey, T. L., Church, G. M., De Moor, B., Eskin, E., Favorov, A. V., Frith, M. C., Fu, Y., Kent, W. J., et al. Assessing computational tools for the discovery of transcription factor binding sites. *Nature Biotechnology*, 23(1):137–144, 2005.
- Touvron, H., Lavril, T., Izacard, G., Martinet, X., Lachaux, M.-A., Lacroix, T., Rozière, B., Goyal, N., Hambro, E., Azhar, F., et al. Llama: Open and efficient foundation language models. *arXiv preprint arXiv:2302.13971*, 2023.
- Van Den Oord, A., Vinyals, O., et al. Neural discrete representation learning. *Advances in neural information processing systems*, 30, 2017.
- Van Roey, K., Gibson, T. J., and Davey, N. E. Motif switches: decision-making in cell regulation. *Current opinion in structural biology*, 22(3):378–385, 2012.
- Vaswani, A. Attention is all you need. *Advances in Neural Information Processing Systems*, 2017.
- Wang, N., Bian, J., Li, Y., Li, X., Mumtaz, S., Kong, L., and Xiong, H. Multi-purpose rna language modelling with motif-aware pretraining and type-guided fine-tuning. *Nature Machine Intelligence*, pp. 1–10, 2024.
- Wei, J., Wang, X., Schuurmans, D., Bosma, M., Xia, F., Chi, E., Le, Q. V., Zhou, D., et al. Chain-of-thought prompting elicits reasoning in large language models. *Advances in neural information processing systems*, 35:24824–24837, 2022.
- Xin, H., Guo, D., Shao, Z., Ren, Z., Zhu, Q., Liu, B., Ruan, C., Li, W., and Liang, X. Deepseek-prover: Advancing theorem proving in llms through large-scale synthetic data. *arXiv preprint arXiv:2405.14333*, 2024.
- Yadav, C. and Bottou, L. Cold case: The lost mnist digits. *Advances in neural information processing systems*, 32, 2019.
- Yang, Y., Gomez, N., Infarinato, N., Adam, R. C., Sribour, M., Baek, I., Laurin, M., and Fuchs, E. The pioneer factor

sox9 competes for epigenetic factors to switch stem cell fates. *Nature Cell Biology*, 25(8):1185–1195, 2023.

Zhang, B. and Sennrich, R. Root mean square layer normalization. *Advances in Neural Information Processing Systems*, 32, 2019.

Zheng, J., Qiu, S., Shi, C., and Ma, Q. Towards lifelong learning of large language models: A survey. *arXiv preprint arXiv:2406.06391*, 2024.

Zhou, J. and Troyanskaya, O. G. Predicting effects of noncoding variants with deep learning–based sequence model. *Nature methods*, 12(10):931–934, 2015.

Zhou, Z., Ji, Y., Li, W., Dutta, P., Davuluri, R., and Liu, H. Dnabert-2: Efficient foundation model and benchmark for multi-species genome. *arXiv preprint arXiv:2306.15006*, 2023.

A. Pretraining Model Configurations

The family of Omni-DNA has six models, and their parameters and architectures are shown in Table 6 and Table 7.

Table 6. Architecture for 6 Omni-DNA models.

Parameters	Layers	Heads	d_{model}	LayerNorm
20M	8	8	256	RMS
60M	8	8	512	RMS
116M	12	12	768	No Bias
300M	16	16	1024	RMS
700M	16	16	1536	RMS
1B	16	16	2048	No Bias

Table 7. Comparison of pretraining setup between Omni-DNA, DNABERT2, and NT-transformer.

	Omni-DNA (six sizes)	DNABERT2 (116M)	NT-transformer (5 sizes)
Layer norm type	non-parametric/RMSNorm	parametric	parametric
Positional embeddings	RoPE	ALiBi	RoPE
Attention variant	full	full	full
Biases	none	in both LN and Attention	in both LN and Attention
Block type	sequential	sequential	sequential
Activation	SwiGLU	GEGLU	SwiGLU
Sequence length (In Tokens)	250	128	1000
Batch size (Across GPUs)	384	4096	512
Total Steps	800000	150000	16,000
Warmup steps	5000	-	16,000
Peak LR	3.0E-04	5.0E-04	1.0E-04
Minimum LR	3.0E-05	0	5.0E-05
Weight decay	0.1	1e-5	0.1
Beta1	0.9	0.9	0.9
Beta2	0.95	0.98	0.999
Epsilon	1.0E-05	1.0E-05	1.0E-08
LR schedule	linear	linear	linear
Gradient clipping	global 1.0	-	-
Training Precision	Mxied (bf16 for most operations)	-	-
Training Framework	Pytorch Built-in FSDP	Pytorch HuggingFace trainer	-
Training Duration (min)	8 GPUs* 1 days	8GPUs * 14 days	128 GPUs*1days
Training Duration (max)	8 GPUs* 7 days	8GPUs * 14 days	128 GPUs*28days
GPU Types	A100 Nvidia GPU 40GB	Nvidia RTX 2080Ti GPUs.	A100 Nvidia GPU

B. Task-specific Nucleotide Transformer Benchmark Results

We present the detailed task-specific results for NT-Downstream tasks in Table 8 and Table 9.

C. Detailed Deduplication Process

C.1. Handling Non-{A, T, G, C} Characters

The raw genome data from the reference genome includes additional characters beyond {A, T, G, C}, which represent ambiguities or gaps. These characters are defined as follows:

- **N**: Represents any nucleotide (A, T, G, or C).
- **R**: Represents purines (A or G).

Table 8. Comparison of Pretraining Models and Fine-tuning Performance Across Tasks (Part 1)

Metric	CADUCEUS-PH	CADUCEUS-PS	DNABERT2 [13]	NT50M	NT100M	NT250M	NT500M	NT2.5B	HyenaDNA
H3	0.815 ± 0.048	0.799 ± 0.029	0.785 ± 0.033	0.745 ± 0.061	0.787 ± 0.010	0.789 ± 0.052	0.784 ± 0.047	0.814	0.779 ± 0.037
H3K14AC	0.631 ± 0.026	0.541 ± 0.212	0.516 ± 0.028	0.471 ± 0.067	0.495 ± 0.101	0.486 ± 0.012	0.551 ± 0.021	0.550	0.612 ± 0.065
H3K36ME3	0.601 ± 0.129	0.609 ± 0.109	0.591 ± 0.020	0.520 ± 0.054	0.557 ± 0.033	0.571 ± 0.011	0.625 ± 0.013	0.632	0.613 ± 0.041
H3K4ME1	0.523 ± 0.039	0.488 ± 0.102	0.511 ± 0.028	0.442 ± 0.021	0.479 ± 0.047	0.486 ± 0.011	0.550 ± 0.021	0.559	0.512 ± 0.024
H3K4ME2	0.487 ± 0.170	0.388 ± 0.101	0.336 ± 0.040	0.224 ± 0.011	0.261 ± 0.042	0.299 ± 0.017	0.319 ± 0.045	0.326	0.455 ± 0.095
H3K4ME3	0.544 ± 0.045	0.440 ± 0.202	0.352 ± 0.077	0.294 ± 0.011	0.336 ± 0.033	0.360 ± 0.033	0.410 ± 0.033	0.421	0.549 ± 0.056
H3K79ME3	0.697 ± 0.077	0.676 ± 0.026	0.613 ± 0.030	0.544 ± 0.016	0.565 ± 0.089	0.591 ± 0.020	0.626 ± 0.026	0.642	0.672 ± 0.048
H3K9AC	0.622 ± 0.030	0.604 ± 0.048	0.542 ± 0.029	0.489 ± 0.011	0.544 ± 0.021	0.552 ± 0.035	0.562 ± 0.040	0.575	0.581 ± 0.061
H4	0.811 ± 0.022	0.789 ± 0.020	0.796 ± 0.027	0.784 ± 0.061	0.707 ± 0.060	0.773 ± 0.013	0.799 ± 0.025	0.822	0.763 ± 0.044
H4AC	0.621 ± 0.054	0.525 ± 0.240	0.463 ± 0.041	0.417 ± 0.051	0.443 ± 0.008	0.454 ± 0.061	0.495 ± 0.032	0.501	0.564 ± 0.038
Enhancer	0.546 ± 0.073	0.491 ± 0.066	0.516 ± 0.098	0.514 ± 0.004	0.515 ± 0.004	0.519 ± 0.028	0.548 ± 0.144	0.580	0.517 ± 0.117
Enhancer Types	0.439 ± 0.054	0.416 ± 0.095	0.423 ± 0.051	0.415 ± 0.092	0.435 ± 0.003	0.426 ± 0.031	0.424 ± 0.132	0.474	0.386 ± 0.185
Promoter: ALL	0.970 ± 0.004	0.967 ± 0.004	0.971 ± 0.006	0.959 ± 0.017	0.967 ± 0.132	0.972 ± 0.008	0.976 ± 0.006	0.974	0.960 ± 0.005
Promoter: NONTATA	0.969 ± 0.011	0.968 ± 0.006	0.972 ± 0.005	0.956 ± 0.010	0.967 ± 0.045	0.973 ± 0.010	0.976 ± 0.005	0.977	0.959 ± 0.008
Promoter: TATA	0.953 ± 0.016	0.957 ± 0.015	0.955 ± 0.021	0.946 ± 0.041	0.937 ± 0.032	0.960 ± 0.03	0.966 ± 0.013	0.964	0.944 ± 0.040
Splice All	0.940 ± 0.027	0.927 ± 0.021	0.939 ± 0.009	0.978 ± 0.016	0.986 ± 0.090	0.979 ± 0.071	0.983 ± 0.008	0.983	0.956 ± 0.011
Splice Acceptor	0.937 ± 0.033	0.936 ± 0.077	0.975 ± 0.006	0.981 ± 0.004	0.979 ± 0.033	0.985 ± 0.068	0.981 ± 0.011	0.990	0.958 ± 0.010
Splice Donor	0.948 ± 0.025	0.874 ± 0.289	0.963 ± 0.006	0.981 ± 0.078	0.983 ± 0.043	0.985 ± 0.091	0.985 ± 0.022	0.984	0.949 ± 0.024
#Params	1.9M	1.9M	150M	50M	100M	250M	500M	2.5B	1.6M

Table 9. Comparison of Pretraining Models and Fine-tuning Performance Across Tasks (Part 2)

Metric	OLMo-DNA20M	OLMo-DNA60M	OLMo-DNA116M	OLMo-DNA300M	OLMo-DNA700M	OLMo-DNA1B
H3	0.778 ± 0.022	0.775 ± 0.022	0.818 ± 0.005	0.820 ± 0.005	0.813 ± 0.019	0.824 ± 0.032
H3K14AC	0.514 ± 0.043	0.566 ± 0.050	0.685 ± 0.014	0.639 ± 0.010	0.672 ± 0.031	0.697 ± 0.077
H3K36ME3	0.525 ± 0.16	0.525 ± 0.019	0.661 ± 0.013	0.648 ± 0.010	0.689 ± 0.096	0.686 ± 0.002
H3K4ME1	0.393 ± 0.016	0.400 ± 0.085	0.577 ± 0.083	0.543 ± 0.076	0.577 ± 0.101	0.617 ± 0.000
H3K4ME2	0.382 ± 0.110	0.407 ± 0.041	0.576 ± 0.003	0.515 ± 0.007	0.568 ± 0.025	0.547 ± 0.006
H3K4ME3	0.435 ± 0.190	0.298 ± 0.181	0.587 ± 0.222	0.628 ± 0.120	0.584 ± 0.076	0.642 ± 0.001
H3K79ME3	0.588 ± 0.008	0.655 ± 0.011	0.718 ± 0.027	0.707 ± 0.028	0.730 ± 0.087	0.752 ± 0.007
H3K9AC	0.525 ± 0.027	0.559 ± 0.023	0.658 ± 0.029	0.652 ± 0.031	0.663 ± 0.051	0.701 ± 0.002
H4	0.756 ± 0.035	0.795 ± 0.091	0.802 ± 0.002	0.786 ± 0.014	0.793 ± 0.045	0.822 ± 0.005
H4AC	0.485 ± 0.059	0.538 ± 0.047	0.663 ± 0.029	0.659 ± 0.019	0.656 ± 0.014	0.652 ± 0.001
Enhancer	0.511 ± 0.049	0.558 ± 0.074	0.593 ± 0.005	0.545 ± 0.006	0.596 ± 0.010	0.580 ± 0.018
Enhancer Types	0.457 ± 0.014	0.511 ± 0.117	0.498 ± 0.001	0.426 ± 0.004	0.443 ± 0.062	0.492 ± 0.023
Promoter: ALL	0.962 ± 0.001	0.962 ± 0.008	0.973 ± 0.002	0.972 ± 0.003	0.971 ± 0.006	0.973 ± 0.001
Promoter: NONTATA	0.964 ± 0.006	0.964 ± 0.007	0.972 ± 0.016	0.973 ± 0.021	0.975 ± 0.005	0.975 ± 0.001
Promoter: TATA	0.945 ± 0.016	0.945 ± 0.017	0.967 ± 0.001	0.961 ± 0.027	0.956 ± 0.016	0.973 ± 0.002
Splice All	0.835 ± 0.145	0.835 ± 0.014	0.927 ± 0.025	0.940 ± 0.016	0.948 ± 0.026	0.941 ± 0.003
Splice Acceptor	0.931 ± 0.001	0.930 ± 0.003	0.968 ± 0.002	0.970 ± 0.009	0.968 ± 0.018	0.972 ± 0.001
Splice Donor	0.927 ± 0.023	0.927 ± 0.023	0.951 ± 0.007	0.957 ± 0.091	0.961 ± 0.031	0.963 ± 0.001
#Params	20M	60M	116M	300M	700M	1B

- **Y**: Represents pyrimidines (C or T).
- Other characters (e.g., **W, S, K, M**, etc.) represent specific nucleotide subsets or unknown bases.

These characters were removed during preprocessing to retain only the core nucleotide sequences ($\{A, T, G, C\}$), ensuring consistency and facilitating the deduplication process.

C.2. Chunk-Based Deduplication

The deduplication procedure was performed as follows:

1. **Chunking**: The genome was divided into non-overlapping chunks of 1024 base pairs.
2. **Exact Matching**: Identical sequences across the dataset were identified and removed.
3. **Efficiency**: This step utilized hashing techniques and optimized string comparison algorithms to handle the large dataset efficiently.

C.3. Results

The raw genome dataset initially contained approximately 170 billion nucleotides. After applying the deduplication process, the dataset was reduced to 30 billion nucleotides, representing unique sequences across multiple species.

C.4. Rationale for Multiple Epochs

Although deduplication significantly reduced the size of the dataset, the smaller dataset was iterated over multiple epochs during pretraining. This approach ensured that repeated sequences were temporally separated during the training process. By maximizing the temporal distance between occurrences of the same sequence, the risk of overfitting was mitigated, leading to better generalization performance.

D. Finetuning with Classification Head

Basic Setup We closely follow the setup from Caduceus (Schiff et al., 2024) for evaluating Omni-DNA. The following models are compared: Omni-DNA, DNABERT-2 (Zhou et al., 2023), NT-Transformer (Dalla-Torre et al., 2024), HyenaDNA (Nguyen et al., 2024), and the Caduceus models (Schiff et al., 2024).

For NT Downstream tasks, we use a maximum fine-tuning epoch of 20, while for the Genomic Benchmark (GB) tasks, we use a maximum of 10 epochs. Both NT Downstream and GB tasks include a training set and a test set. For hyperparameter search, 10% of the training set is reserved as a validation set.

Hardware & Framework All fine-tuning is conducted on a single NVIDIA A100 40GB GPU. We utilize the Hugging Face Trainer API for full-size fine-tuning of the pretrained checkpoints. Models are loaded using the `AutoModelForSequenceClassification` class, which automatically adds a linear layer on top for sequence classification.

Our experimental results align with those reported in Caduceus (Schiff et al., 2024). For consistency, we report statistics from (Schiff et al., 2024) for two Caduceus models, DNABERT-2, NT-Transformer 500M, and HyenaDNA in NT Downstream tasks, as well as CNN, HyenaDNA, and CADUCEUS-PH in GB tasks. For NT2.5B, we use the results from its original paper (Dalla-Torre et al., 2024).

We replicate experiments for the following models: NT50M, NT100M, NT250M, along with six Omni-DNA models on 18 NT Downstream tasks. Additionally, we fine-tune DNABERT-2 and Omni-DNA 116M on the eight Genomic Benchmark tasks.

Hyperparameters A simple grid search is performed for each model using hyperparameters provided in Table 10.

Table 10. Finetuning hyperparameters.

Hyperparameter	Value
Peak learning rate	$[3 \times 10^{-4}, 1 \times 10^{-5}, 5 \times 10^{-6}]$
Per device train batch size	[8,16,32]
Max gradient norm	1.0
Weight decay	0.1
Adam β_1	0.9
Adam β_2	0.999
Adam ϵ	1×10^{-8}
Optimizer	ADAMW

Additional Notes We observe a performance gap in HyenaDNA between our replication results, which align with those of (Schiff et al., 2024), and the results reported in the original paper (Nguyen et al., 2024), both on NT downstream and GB tasks. Our replication follows our own setup, yielding results consistent with (Schiff et al., 2024). Upon reviewing the code within the container image provided by (Nguyen et al., 2024), we identified additional techniques such as Exponential Moving Average (EMA) and data augmentation that were employed, which may account for the discrepancy. In this work, we use HyenaDNA results obtained without these techniques as the baseline.

E. Needles in a DNA

For random DNA sequence generation, we use the Expectation-Maximization (EM) algorithm implemented in the Python package `hmmlearn` to train a Hidden Markov Model (HMM) with two states, learning both the transition and emission probabilities. We then insert one of the functional motifs from {TATAAA, CAAT, GGGCGG, TTAGGG} into the randomly generated sequences. Finally, we filter the sequences, preserving only those that contain exactly one instance of a motif. We generate 12,000 sequences for each motif type.

Next, we process the MNIST images through a trained Vector Quantized Variational Autoencoder (VQ-VAE) to obtain discretized token representations corresponding to each motif type. The pretraining and architecture details of the VQ-VAE are described in the following section.

E.1. VQ-VAE

To learn discrete representations of image features, we employ a Vector Quantized Variational Autoencoder (VQ-VAE), which consists of an encoder, a vector quantization layer, and a decoder.

E.1.1. ENCODER

The encoder transforms input images into a latent space representation. It is implemented as a convolutional neural network (CNN) with residual connections. The architecture consists of:

- An initial 4×4 convolution with stride 2 and padding 1, reducing the spatial dimensions while increasing feature depth.
- A second 4×4 convolution with stride 2, further downsampling the input.
- A 3×3 convolution maintaining the number of hidden channels.
- A residual stack of multiple layers with 3×3 and 1×1 convolutions, enhancing feature extraction.

The output of the encoder is then passed through a 1×1 convolution to adjust the feature dimensionality before quantization.

E.1.2. VECTOR QUANTIZATION

The latent representations are discretized using vector quantization, which maps continuous encodings to the nearest prototype in a learned codebook. We use two different approaches:

- The standard VQ-VAE, where the codebook is learned via backpropagation.

- The exponential moving average (EMA) variant, which updates the codebook using an EMA of past embeddings to stabilize training.

Given a latent representation z_e , the closest embedding vector z_q is selected based on the Euclidean distance. The loss function includes a commitment loss term, weighted by a hyperparameter β , ensuring that encoded representations stay close to their assigned embedding vectors.

E.1.3. DECODER

The decoder reconstructs the input from the discretized representation. It mirrors the encoder with transposed convolutions for upsampling:

- A 3×3 convolution to process the quantized representation.
- A residual stack for improved reconstruction.
- Two transposed convolutions (4×4 , stride 2) to upsample back to the original image size.

E.1.4. TRAINING AND HYPERPARAMETERS

We train the VQ-VAE using the Adam optimizer with a learning rate of 5×10^{-4} . The following hyperparameters are used:

- Number of hidden channels: 128
- Number of residual layers: 2
- Number of residual hidden units: 32
- Codebook size: 6
- Embedding dimension: 32
- Commitment cost (β): 0.25
- Decay factor (for EMA variant): 0.99

The reconstruction loss is measured using mean squared error (MSE), and training is monitored with additional metrics such as perplexity and codebook usage. The trained VQ-VAE is used to convert MNIST images into discrete tokens, which are then linked to DNA motifs for downstream analysis.



Figure 9. Images Generated by Omni-DNA. These digits are novel in the sense that they do not exist in the training set.

F. Functional Annotation Generation

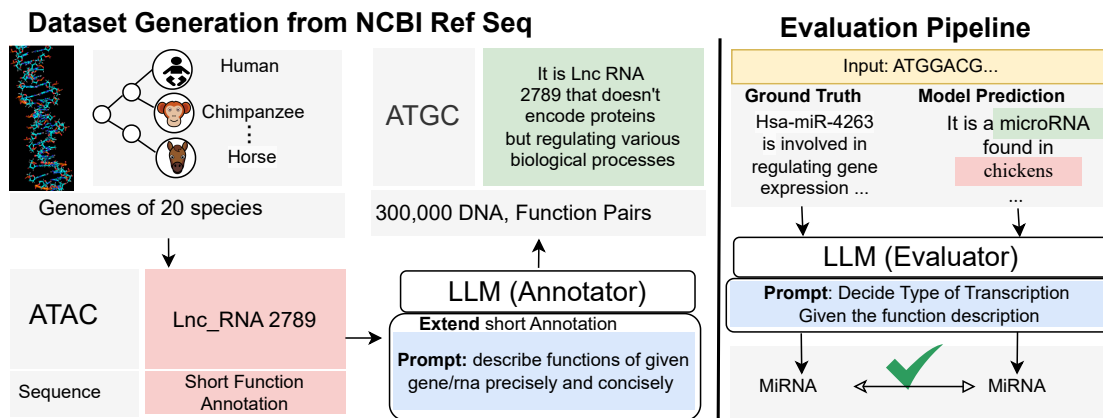


Figure 10. Seq2Func Dataset Construction and Evaluation Pipeline. Genomic sequences from 20 species are annotated with functional descriptions using an LLM, generating 300,000 DNA-function pairs. The evaluation pipeline compares model predictions against ground truth, with an LLM determining transcription type accuracy.

Dataset Construction Process The Seq2Func dataset is constructed using genomic sequences sourced from the **NCBI Reference Sequence (RefSeq)** database, incorporating sequences from **20 different species**. The selected species and their genome assemblies include:

- GCF-000001405.40, human
- GCF-000001635.27, mouse
- GCF-036323735.1, rat
- GCF-028858775.2, Chimpanzee

- GCF-018350175.1, cat
- GCF-011100685.1, dog
- GCF-000696695.1, burgud
- GCF-000003025.6, pig
- GCF-016772045.2, sheep
- GCF-016699485.2, chicken
- GCF-025200985.1, fly
- GCF-000002035.6, Zebrafish
- GCF-029289425.2, Pygmy Chimpanzee
- GCF-029281585.2, Western gorilla
- GCF-028885655.2, Pongo abelii
- GCF-028885625.2, Bornean orangutan
- GCF-003339765.1, Rhesus monkey
- GCF-037993035.1, Macaca fascicularis
- GCF-003668045.3, Chinese hamster
- GCF-041296265.1, horse

The construction process follows these key steps:

Sequence Extraction and Functional Annotation

- The raw dataset includes a diverse set of RNA sequences with different functional annotations.
- The original dataset consists of the following RNA types and their counts:
 - mRNA: 220397
 - tRNA: 20674
 - snRNA: 18996
 - snoRNA: 15577
 - lncRNA: 14291
 - miRNA: 12238
 - primary-transcript: 8644
 - rRNA: 6225
 - transcript: 3860
 - ncRNA: 477
 - guide-RNA: 143
 - antisense-RNA: 28
 - RNase-P-RNA: 9
 - V-gene-segment: 7
 - scRNA: 7
 - Y-RNA: 6
 - telomerase-RNA: 5

- vault-RNA: 4
- SRP-RNA: 4
- RNase-MRP-RNA: 3
- C-gene-segment: 2
- D-gene-segment: 1
- To refine the dataset, only **seven functional RNA types** are retained:
 - mRNA
 - tRNA
 - snRNA
 - snoRNA
 - lncRNA
 - miRNA
 - rRNA

Annotation Enhancement Using a Large Language Model (LLM)

- A **LLM Annotator** is employed to extend and refine functional annotations.
- The model is prompted with: *Describe the functions of the given gene/RNA precisely and concisely.*
- For example, an initial annotation like Lnc RNA 2789” is expanded into:

“It is Lnc RNA 2789 that doesn’t encode proteins but regulates various biological processes.”

Final Dataset Composition

- The final dataset consists of **300,000 DNA-function pairs**, where each DNA sequence is paired with an enhanced functional description.
- These functionally annotated sequences serve as high-quality input for machine learning models.

Usage	Prompt
Used by LLM (Annotator) for extending the short annotation to detailed function annotation	(System Prompt) You are a helpful assistant that answers functions of given gene/rna precisely and concisely.
Used by LLM (Evaluator) for deciding the type of DNA given its function description	(System Prompt) You are a helpful assistant that determines the type of RNA based on the given function description. When deciding the functoin. Your answer should to only be one of the ['mRNA', 'tRNA', 'snRNA', 'snoRNA', 'lncRNA', 'miRNA', 'rRNA']
Given to GPT4o@zeroshot for performing zeroshot DNA function prediction	(System Prompt) You are a helpful assistant that determines the type of RNA based on the given DNA sequence. Your answer should only be one of the mRNA, tRNA, snRNA, snoRNA, lncRNA, miRNA, rRNA

Table 11. Prompt Used during dataset construction, evaluation and zeroshot prediction

Ground Truth	GPT4o	Olmo@ft	OmniDNA@ft
(Input) TGGCAGAGATATG...AAGAAAAAAGAAAATGAACTTGGTGCAGGCA (DNA of length 1000)			
<p>mRNA:CD209, also known as DC-SIGN (Dendritic Cell Specific Intercellular adhesion molecule-3-grabbing Nonintegrin), is a type I transmembrane protein primarily expressed on dendritic cells and some other immune cells. It functions as a receptor that binds and internalizes pathogens, including viruses and bacteria, thereby facilitating their presentation to T cells and playing a critical role in the immune response. CD209 is involved in the recognition of mannose-rich ligands, mediating cellular adhesion, and influencing various aspects of immune activation and tolerance. Additionally, it can modulate inflammatory responses and has been implicated in HIV-1 and other pathogen infections.</p>	<p>The provided DNA sequence likely represents a genomic region involved in regulatory or coding functions. Based on its composition, it may contain promoter elements, coding regions, untranslated regions (UTRs), or repetitive sequences.</p>	<p>The mRNA for the putative POM121-like protein 1-like likely encodes a protein that is similar to POM121, which is a component of the nuclear pore complex. This protein may play a role in nucleocytoplasmic transport, facilitating the movement of molecules between the nucleus and cytoplasm. The "putative" designation suggests that its function is inferred from homology to other known proteins, but it may not yet be fully characterized in terms of its specific biological roles or mechanisms.</p>	<p>C-C motif chemokine ligand 22 (CCL22) is a chemokine involved in immune responses . It primarily attracts and activates T cells , particularly regulatory T cells (Tregs), and plays a role in modulating inflammation and immune responses . CCL22 is produced by various cell types , including macrophages and dendritic cells , and is implicated in various diseases , including autoimmune disorders and cancer.</p>

Table 12. Comparison of Ground Truth, GPT4o, Olmo@ft, and OmniDNA@ft in RNA type determination (Example 1)

Ground Truth	GPT4o	Olmo@ft	OmniDNA@ft
(Input) GAGGTAGTAGATTGTATAG			
<p>miR -3596d is a microRNA found in rats (<i>Rattus norvegicus</i>). It is involved in the regulation of gene expression at the post-transcriptional level, primarily by binding to complementary sequences in messenger RNAs (mRNAs), leading to their degradation or inhibition of translation. While specific target genes may vary, miRNAs like rno-miR-3596d generally play roles in various biological processes such as development, cell differentiation, proliferation, and apoptosis. Specific roles or targets for rno-miR-3596d would require experimental validation or further studies to elucidate its functions in rat biology.</p>	<p>The DNA sequence GAGGTAGTAGATTGTATAG could serve various functions depending on its genomic context. Generally, it could be: 1. A regulatory element – If found in promoter or enhancer regions, it may influence gene expression. 2. A binding site – It could be a recognition site for transcription factors, such as ETS-family proteins (which recognize GGAA/T motifs). 3. A coding or non-coding region – If within a gene, it might encode a peptide or function as a non-coding RNA. 4. A structural or repeat element – It could contribute to chromatin organization or genome stability. For precise functional annotation, its location within a genome and experimental validation would be needed.</p>	<p>hsa-miR-4684 is a microRNA (miRNA) found in humans. It is involved in the regulation of gene expression by binding to complementary sequences in target messenger RNAs (mRNAs), leading to their degradation or inhibition of translation. miR-4684 may play roles in various biological processes, including development, cell proliferation, and differentiation. Specific target genes and pathways regulated by hsa-miR-4684 may vary, and ongoing research aims to elucidate its precise functions</p>	<p>gga - miR - 65 77 - 5p is a microRNA (miRNA) found in chickens (<i>Gallus gallus</i>). MicroRNAs are small , non - coding RNA molecules that play a crucial role in regulating gene expression by binding to complementary sequences on target messenger RNAs (mRNAs), leading to their degradation or inhibition of translation . Specifically , gga - miR - 65 77 - 5p may be involved in various biological processes , including development , differentiation , and response to stress , although specific target genes and functions may require further study</p>

Table 13. Comparison of Ground Truth, GPT4o, Olmo@ft, and OmniDNA@ft in RNA type determination (Example 2)

Ground Truth	GPT4o	Olmo@ft	OmniDNA@ft
(Input) TGCTCACTTCAGCAGCACATGTGCTAAAAT TGGAATGACACAAAGAAGATTAGCATGGCCGC TGAGCAAGGATGACACGCACATTTGTGAATTGTTCCATAAAAAA			
<p>nRNA:U6 spliceosomal RNA is a small nuclear RNA (snRNA) that plays an essential role in the splicing of pre-mRNA in eukaryotic cells. It is a core component of the spliceosome, the complex responsible for the removal of introns from pre-mRNA transcripts. U6 engages in base-pairing interactions with other spliceosomal RNAs and pre-mRNA, facilitating the assembly and function of the spliceosome. Its primary roles include catalyzing the cleavage of introns and the ligation of exons during the splicing process. U6 is also involved in the activation of the catalytic core of the spliceosome, making it crucial for proper gene expression.</p>	<p>The given DNA sequence likely encodes a functional genetic element, such as a protein-coding region or a regulatory sequence. To determine its precise function, I will need to analyze it for potential coding regions, motifs, or regulatory elements.</p>	<p>U6 spliceosomal RNA is a small nuclear RNA (snRNA) that plays a crucial role in the splicing of pre-mRNA in eukaryotic cells. It is a core component of the spliceosome, the complex responsible for removing introns from pre-mRNA transcripts. U6 RNA is involved in the catalysis of the splicing reaction and helps in the formation of the active site of the spliceosome, facilitating the precise excision of introns and the ligation of exons.</p>	<p>U6 spliceosomal RNA is a small nuclear RNA (snRNA) that plays a crucial role in the splicing of pre - mRNA in eukaryotic cells . It is a component of the spliceosome , the complex responsible for removing introns from pre - mRNA and joining exons together . U6 RNA is involved in the catalytic activity of the spliceosome and is essential for the recognition of splice sites and the formation of the active site for splicing . It also interacts with other snRNAs.</p>

Table 14. Comparison of Ground Truth, GPT4o, Olmo@ft, and OmniDNA@ft in RNA type determination (Example 3)